Green Chemistry

PAPER

View Article Online
View Journal | View Issue

Cite this: *Green Chem.*, 2025, **27**, 9578

Leaching state prediction for battery black mass using online sensor data†

Wei Song, *[a] Andrey Yasinskiy,[a] Fabian Diaz,[a] Tobias Kleinert[b] and Bernd Friedrich [a]

Received 2nd February 2025,
Accepted 4th June 2025

DOI: 10.1039/d5gc00581g

rsc.li/greenchem

This study investigates the leaching behavior of metal elements from pyrolyzed battery black mass using a combination of experimental and data analysis methods. A linear regression model, utilizing pH, conductivity, and temperature as input features, effectively predicted leaching states with an average prediction error below 1.1%. Compared to calculating leaching states using the Arrhenius equation and traditional kinetic models, the proposed approach demonstrated improved generalizability and accuracy. Kinetic analysis using the shrinking core model indicated that the leaching of nickel and cobalt is primarily controlled by diffusion after an initially chemically controlled reaction phase. This diffusion-controlled mechanism explains the observed strong linear relationship between sensor data and the leaching states of these metals. The calculated activation energies for nickel and cobalt are 29.8 kJ mol^{-1} and 22.6 kJ mol^{-1}, respectively. The rapid leaching kinetics of lithium and manganese are attributed to their unique physiochemical properties, likely influenced by the thermal treatment process.

Green foundation

1. This study proposes a new approach for predicting the leaching state using easily measurable online sensor data. Compared to leaching kinetic models, this approach enhances model generalizability by considering the dynamic conditions of a new process and providing timely feedback for potential process optimization.
2. The leaching state of Al, Fe, Ni, Co, Li, and Mn can be accurately predicted using a multiple linear regression model with pH, conductivity, and temperature as input features. The model demonstrated an average adjusted *R*-squared score of 0.995 and an average prediction error of 1.1%.
3. The proposed method avoids the need for complex material characteristics and structural limitations and provides valuable insights for online process monitoring by predicting leaching state using sensor data. Advanced methods such as machine learning can be applied to simply the process and address more complex scenarios in future research.

1 Introduction

Hydrometallurgy is an extractive metallurgical technique and has been widely used to recycle valuable components from spent lithium-ion batteries (LIBs) with various aqueous solutions.[1] Leaching, frequently the initial step of hydrometallurgical processes, selectively dissolves target metals from solid matrix into a liquid phase using a leaching agent. This process is crucial for extracting valuable metals from both primary and secondary materials. Inorganic acids, such as sulfuric acid and hydrochloric acid, have been used to leach battery cathode materials, as hydrogen ions facilitate lithium extraction from spent LIBs.[2] Organic acids, such as citric acid and ascorbic acid, have less environmental impact and serve as alternative leaching agents for battery recycling. Hydrogen peroxide (H_2O_2) is commonly used as a reductant in black mass leaching, and its influence has been investigated in many studies.[3–5]

Thermodynamics and kinetics are fundamental for understanding the leaching mechanisms. Thermodynamics analyzes the directions, energies, products, and equilibrium conditions of chemical reactions, but it does not consider the time factor. Conversely, kinetics considers time changes and thus provides a more realistic explanation of leaching phenomena.[6] The chemical reaction rate, which describes the progress of a reaction, can be expressed as a function of conversion. Kinetic studies interpret reaction mechanisms by examining the influence of experimental conditions on the reaction rate. This understanding is crucial for process control, optimization, and

[a]*IME Process Metallurgy and Metal Recycling, Institute of RWTH Aachen University, Intzestr. 3, 52056 Aachen, Germany. E-mail: wsong@ime-aachen.de*
[b]*Chair of Information and Automation Systems for Process and Material Technology, RWTH Aachen University, 52064 Aachen, Germany*

† Electronic supplementary information (ESI) available. See DOI: https://doi.org/10.1039/d5gc00581g

reactor design. As leaching is often the initial step in hydrometallurgical processes, comprehending its mechanisms is essential.[7] Specifically, in battery recycling, the leaching kinetics of critical metals (*e.g.* Ni, Mn, Co, and Li) from black mass is a key consideration for industrial-scale recycling.[8]

Various mathematical models simplify kinetic investigations of heterogeneous reactions.[9,10] Reuter *et al.* employed a generalized neural-net kinetic rate equation to simulate a metallurgical and mineral processing system and identify optimal process conditions.[11] In leaching kinetic modeling, the progressive conversion model (PCM) is a simple approach used to predict leaching completion time. It assumes a constant particle size and is applicable when the diffusion rate through the particle's pores is high. The shrinking core model (SCM), which accounts for changes in solid material structure and surface area, offers a more realistic representation of solid–liquid reactions and is the most commonly used model for leaching kinetics.[6] For homogeneous nucleation, the Avrami model can also be applied.[12,13] These models provide simplified analytical solutions for complex reactions.[6]

Correlation analysis is a valuable tool in experimental research. It helps identify and quantify the relationship between variables, providing insight into the strength and direction of the data relationship.[14] Correlation analysis efficiently determines linear and monotonic relationships, serving as a fundamental step in developing forecasting models. By examining the potential to predict one variable with another, research can gain valuable insights.[15–17] Correlation analysis can also be used for validation purposes by assessing the agreement between two measurement methods.[18] The coefficient of determination (R^2) quantifies the difference between predicted and experimental data, and is widely used to evaluate the performance of regression models.[19–21] However, relying solely on correlation coefficient is insufficient and can cause misinterpretation. It is essential to employ additional analysis methods that highlight differences between pairs of observations.[22] Correlation analysis is frequently combined with kinetics analysis to optimize experimental conditions. By evaluating the correlation between process parameters and outcomes, researchers can identify optimal settings. Furthermore, correlation and statistical analyses are crucial for selecting and assessing suitable kinetic models.

Table 1 summarizes related studies that have employed kinetic modeling and correlation analysis in leaching processes. For rotating disk electrode experiments, mechanistic kinetic models were developed to study the rate-controlling steps and to estimate the rate of gold dissolution. Correlation analysis revealed that the gold dissolution rate is proportional to temperature and the concentration of either cupric or ferric ions, depending on whether cupric chloride or ferric chloride was used as the leaching agent.[23,24] The leaching kinetics of copper extraction from waste printed circuit boards (WPCBs) can be effectively described using the Avrami model. Multiple linear regression (MLR) analysis was employed to investigate the correlation between experimental conditions and copper leaching efficiency. The results indicated that temperature (T), solid–liquid ratio, and H_2O_2 concentration exert significant effects on the copper leaching efficiency.[25] In the context of scrap magnet recycling, the shrinking core model was utilized to model the kinetics of neodymium dissolution. The overall leaching process was determined to be governed by surface chemical control, with the dissolution rate of neodymium primarily influenced by temperature and acetic acid concentration.[26]

The SCM is also frequently applied to describe the leaching kinetics of spent lithium-ion batteries. Kinetic modeling of cobalt recovery from cathodic powder using nitric acid revealed that the process is controlled by product layer diffusion, whereas cobalt leaching with citric acid is chemically controlled. Notably, temperature and solvent concentration are key parameters significantly influencing cobalt leaching efficiency.[27,28] When leaching battery cathode materials using hydrochloride acid, the dissolution of nickel, manganese, and cobalt (NMC) is controlled by chemical reaction. The dissolution rate of lithium is faster than that of the transition metals. Cathode materials with higher nickel content exhibit faster dissolution rates compared to those with lower nickel content. Both the SCM and a first-order rate law were employed to calculate the time required for complete digestion.[29] A rapid leaching method was developed by using a mixture of hydrochloric acid and ascorbic acid. The SCM, Avrami model, and parabolic product layer diffusion control models were used to interpret the reaction mechanisms. The Pearson's correlation coefficient was employed to quantify the correlations of both reagents to leaching rates.[30] In the sulfuric acid leaching system, ferrous ions serve as an essential reducing agent for cobalt in the recycling of spent LIBs. Iron scrap can be utilized as a cost-effective source of ferrous ions during leaching to enhance cobalt recovery. Kinetic analysis using the SCM indicated that the addition of ferrous ions accelerates metal transfer by mitigating the formation of the ash layer. The results of MLR demonstrated that the pH of the reagent has the most significant impact on the leaching efficiency of lithium and cobalt, followed by ferrous concentration, temperature, and agitation.[31] In addition to iron scrap, industrial black liquor, a by-product of the Kraft pulping process in papermaking, can also be employed as a renewable reducing agent for the leaching of battery black mass with sulfuric acid. A linear correlation was observed between black liquor concentration and the leaching efficiency of manganese. Based on the better fit of diffusion control models and high activation energies, the reaction mechanism for cobalt, nickel, and manganese appears to be a mixed diffusion-reaction process.[32]

Kinetic investigations of leaching can be challenging due to the complexities of data collection and kinetic modeling. Experimental data, particularly leachate concentrations, must be collected over time and analyzed using precise analytical techniques. To facilitate the selection of an appropriate kinetic model, it is essential to characterize the material's structure both before and after leaching operation. Techniques such as transmission electron microscopy (TEM), scanning electron

Table 1 Leaching kinetic models and correlation analysis

Material	Solvent	Kinetic models	Key parameters	Target elements	Correlation analysis	References
Gold	Cupric chloride	Mechanistic kinetic model	*T*, cupric ion concentration	Au	Visual inspection	Lampinen *et al.*[23]
Gold	Ferric chloride	Mechanistic kinetic model	*T*, ferric ion concentration, chloride concentration	Au	Visual inspection	Seisko *et al.*[24]
WPCBs	Sulfuric acid	Avrami model	*T*, solid–liquid ratio, H_2O_2 concentration	Cu	Visual inspection, MLR	Hao *et al.*[25]
Scrap magnet	Acetic acid	SCM	*T*, solvent concentration	Nd	Visual inspection	Behera *et al.*[26]
Spent LIBs	Citric acid	SCM	*T*, solvent concentration	Co, Ni	Visual inspection	Yuliusman *et al.*[28]
Spent LIBs	Hydrochloric acid	SCM, first-order rate law	*T*, type of NMC cathode material	Li, Co, Ni, Mn	Visual inspection	Xuan *et al.*[29]
Spent LIBs	Hydrochloric acid & ascorbic acid	SCM, Avrami model, parabolic product layer diffusion control	*T*, solid–liquid ratio, solvent concentration	Li, Co, Ni, Mn	Visual inspection, Pearson's correlation coefficient	Xing *et al.*[30]
Spent LIBs	Sulfuric acid	SCM	pH, ferrous concentration, *T*, agitation	Li, Co	Visual inspection, MLR	Ghassa *et al.*[31]
Spent LIBs	Sulfuric acid	SCM	*T*, solvent type and concentration, reductant concentration	Co, Ni, Mn	Visual inspection	Carreira *et al.*[32]

microscopy (SEM), and Brunauer–Emmett–Teller (BET) analysis are commonly employed for this purpose.[33–35] Once a kinetic model is developed, it can be used to predict the leaching behavior in subsequent experiments. This prediction is achieved by applying equations that incorporate previously determined kinetic parameters and the specific conditions of the new experiment. However, existing theoretical models and correlation analyses often rely on fixed values for experimental conditions. Consequently, due to the inherent complexity of real-world systems, which frequently involve heterogeneous materials and phase changes, predictions made without considering the dynamic nature of the process may exhibit deviations from actual observed values.[36]

To address the need to consider process dynamics and improve prediction accuracy, in-line sensors can be utilized to capture process parameters during leaching. pH is mathematically defined as the negative logarithm of the hydrogen ion activity. In dilute solutions, the hydrogen ion activity can be simplified and approximated by its concentration, which is influenced by factors such as temperature, dissolved CO_2 levels, and the completion of reactions within the solution.[37] Redox potential indicates a solution's capability for electron transfer. Similar to pH, it represents the ratio of the activities of oxidizing and reducing species within the solution.[38] During acid leaching, alkaline cathode metal oxides react with hydrogen ions, forming soluble metal salts. The change in hydrogen ion concentration within the solution is reflected by pH measurements, while redox potential quantifies the oxidation and reduction activities. Conductivity is mathematically defined as the product of conductance and the cell constant of the measurement cell. A solution's conductivity is dependent on the concentration and electrochemical properties of all dissolved ions. It is also strongly influenced by temperature. Increasing temperature enhances ion mobility, leading to increased conductivity. In binary solutions containing only one electrolyte and water, conductivity can be used as a surrogate for concentration.[39] However, due to the presence of multiple electrolytes in the pregnant leach solution (PLS) derived from battery black mass, conductivity cannot be directly used as a substitution for concentration. Nevertheless, monitoring conductivity can provide valuable real-time insights into the progression of the leaching process and the ion concentrations within the solution. These parameters can be utilized as features of chemical reactions.

In biotechnology, the correlation between redox potential and state variables was investigated during ornithine production. The ornithine concentration can be estimated using online data of redox potential.[40] To study the leaching kinetics of pyrite, May *et al.* developed an experimental technique for on-line redox potential measurement. The relationship between the ferric leach rate of pyrite and measured redox potential was studied qualitatively.[41] In electronic waste recycling, an Arduino program was developed to monitor and control pH and potential within a constant range. This control was implemented to ensure successful leaching of copper, lead, and silver using nitric acid. Furthermore, response surface methodology (RSM) was employed to determine the optimal stirring speed and solid–liquid ratio for maximizing copper leaching efficiency.[42] In battery recycling, researchers monitored pH, potential, and dissolved oxygen concentration during leaching processes to elucidate the fundamental dissolution mechanisms of cathode materials from spent LIBs. The results indicated that the progressive delithiation of the materials is associated with an increase in operating potentials.[30,43]

However, previous studies investigating process behaviors predominantly relied on visual inspection to infer relationships between measured parameters, rather than applying rigorous quantitative correlation analysis.[44] Furthermore, the potential of sensor-derived parameters as reliable indicators of

process progression has not been systematically explored. While techniques such as RSM are widely used for optimizing experimental conditions and guiding design, they are not inherently suited for exploring underlaying data relationships. In contrast, methods like correlation analysis and linear regression offer robust tools for quantifying associations between continuous variables.[14,22] The absence of such quantitative analytical approaches in the context of process monitoring and modeling represents a relevant research gap.

This study aims to effectively track and predict metal leaching states during the sulfuric acid leaching of pyrolyzed battery black mass using online sensor data. Unlike previous work that relied on visual inspection without quantitative correlation analysis, this research employs statistical methods and kinetic models to investigate the relationships between sensor data and metal dissolution.

In this study, pyrolyzed battery black mass was leached with sulfuric acid at varying temperatures. Multiple samples were collected during the leaching process to track the dissolution progress of metal elements. pH, temperature, electrode potential, and conductivity of the leaching solution were monitored continuously. Both sensor data and leaching state are non-fixed variables. The strength and direction of the relationships between these variables were initially investigated through correlation analysis. Subsequently, linear regression models were developed to estimate leaching states based on the online sensor data. The performance of the models was statistically evaluated. The observed linear relationships between online sensor data and metal leaching states were explained by combining kinetic analysis with SCM theory. The activation energies for nickel and cobalt were calculated using the Arrhenius equation. These values were subsequently used, in conjunction with the SCM conversion equations, to determine their respective leaching states. Finally, the morphology and crystal structure of the materials before and after leaching were characterized to support the kinetic analysis.

2 Experimental

2.1 Materials

A commercially vacuum thermally treated black mass (BM) derived from lithium-ion batteries was utilized in this study. The holding temperature during the thermal treatment ranged from 500 to 550 °C. Further details regarding the thermal treatment are proprietary and not disclosed by the company. However, according to the inductively coupled plasma optical emission spectroscopy (ICP-OES) elemental analysis and combustion analysis, the black mass consists of 4.6% aluminum, 1.2% iron, 14.2% nickel, 10.8% cobalt, 4.2% lithium, 9.5% manganese, 2.2% copper, and 27% carbon, as presented in Table 2. The chemical composition suggests that the black mass originated from a blend of various NMC battery cells.

2.2 Leaching experiments

Leaching experiments were conducted using 1 molar sulfuric acid. A charge of 150 grams of pyrolyzed black mass was introduced into a 2-liter double-wall batch reactor and leached for 60 minutes. A solid–liquid ratio of 100 g L^{-1} was maintained throughout experiments. Following the leaching period, the mixture was separated into the undissolved solid residue and the pregnant leach solution by filtration using a paper filter and a vacuum pump.

Table 2 Chemical composition of the utilized battery black mass

Element	Al	Fe	Ni	Co	Li	Mn	Cu	C
g per 100 g BM	4.6	1.2	14.2	10.8	4.2	9.5	2.2	27

To ensure the stability of the experimental data and minimize operational errors, temperature was maintained as the sole variable during the leaching process. Furthermore, to reduce operator-induced variability across experiments, no reducing agents, such as hydrogen peroxide, were employed. This methodology ensured consistency in the results and eliminated potential confounding factors. Eight leaching experiments were conducted, varying the temperature from 25 °C to 75 °C. The temperature was manually set and maintained constant throughout the experiment by a double-wall reactor connected to an external thermostat. During each leaching experiment, 7 mL liquid samples were collected at regular intervals of five minutes using a pipette. For subsequent analysis, solid–liquid separation of these samples was achieved through centrifugation followed by filtration using a syringe filter. Samples collected at 5, 10, 15, 30, and 60 minutes were selected for analysis. Prior to analysis, all collected samples were acidified with HNO_3 and diluted with distilled water at a ratio of 1 : 10. The elemental composition of the diluted samples was then determined using ICP-OES.

In all experiments, a single pH sensor (InPro4260i) and one inductive conductivity sensor (InPro7250), both from Mettler-Toledo GmbH, were used to continuously monitor pH, temperature, electrode potential, and conductivity. The pH sensor provided measurements of pH, temperature, and electrode potential (mV), while the conductivity sensor monitored conductivity. Calibration of the pH sensor was performed using a two-point method with buffer solutions at pH 4 and pH 7. The conductivity sensor was calibrated using a zero-point calibration procedure. The specified measurement accuracies for these parameters were ±0.02 pH, ±0.25 °C, ±1 mV, and ±1%, respectively. Sensor signals were processed by dedicated transmitters before being collected by a datalogger. Data were subsequently transmitted to a measurement laptop *via* serial communication. A custom data acquisition program was developed to visualize and record the sensor data. The complete experimental setup and the measurement devices are illustrated in Fig. 1.

3 Methodology

3.1 Correlation analysis

Current hydrometallurgical battery recycling processes often rely on studies conducted under static conditions. This is

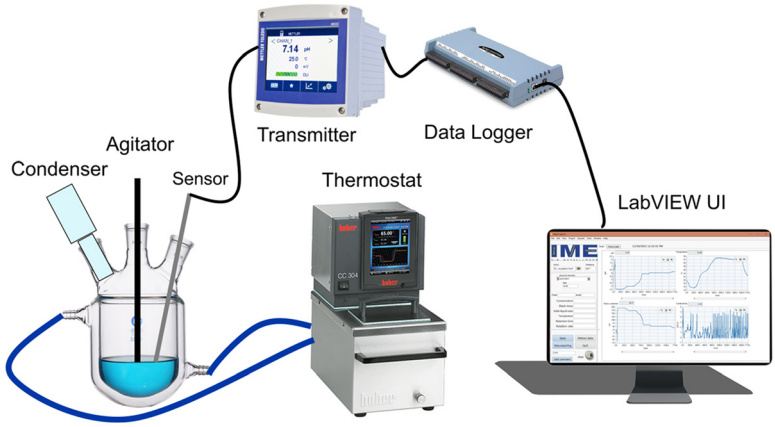

Fig. 1 Experimental setup and measurement devices.

largely due to the inherent complexity of the chemical reactions involved and the typical delay in obtaining comprehensive information about the process state through offline analysis. Online process monitoring, however, offers significant advantages by capturing transient process states, thereby enhancing process transparency and providing deeper insights into underlaying leaching mechanisms. Furthermore, online monitoring facilitates more dynamic and adaptive process control strategies, which can lead to notable advancements in process optimization and innovation.[45]

Given that correlations may exist between parameters such as pH, temperature, electrode potential, and conductivity and the actual leaching states, these online sensor data have potential for estimating leaching progression in real-time. To investigate this potential, a systematic correlation analysis was performed.

As a preliminary step in correlation analysis, the relationships between the metal leaching state and the continuously monitored parameters were visually inspected. An initial focus was placed on the relationship between pH and the leaching state, which was examined using scatter plots. Subsequently, the relationships between all monitored sensor parameters and the leaching state were quantified using correlation coefficients. Since both the sensor data and the metal leaching state are continuous variables, Pearson's correlation coefficient was initially employed to assess the strength and direction of their linear associations. Additionally, Spearman's rank correlation coefficient was calculated to evaluate the strength of monotonic relationships. Compared to Pearson's correlation coefficient, Spearman's is less sensitive to outliers, making it a more robust alternative for analyzing data that may not fully satisfy the assumptions of a linear relationship.

3.2 Multiple linear regression

Linear regression models utilize independent variables to predict dependent variables. In this study, sensor data serve as the independent variables, and used as inputs to the models. While these were treated as independent features for model input, potential relationships among the sensor readings were examined. To mitigate issues arising from multicollinearity, a threshold of 5 was established for the variance inflation factor (VIF). Only combinations of features yielding a VIF below this threshold were utilized in the models. Given that the leaching states of multiple metal elements are described, the linear regression models employed in this study are multivariant linear regression or multiple linear regression.

The primary objective of the regression model was to predict the leaching states of metal elements based on the provided sensor data. However, the inherent complexity of the chemical reactions and the inhomogeneity of the solution posed significant challenges in obtaining consistent sampling results through manual procedures. Variations in sampling time and the dynamic nature of the reaction process could substantially affect the reliability and reproducibility of manually collected data. Consequently, the leaching states inferred from discrete sampling analysis primarily reflected the overall trend of the chemical reactions rather than providing precise, real-time insights. Therefore, linear regression models were utilized to describe this overall trend of the leaching process.

Unlike a purely correlation analysis, the linear regression modeling included data collected from the commencement of the leaching experiments. A total of 46 data points were utilized for modeling the leaching process. Based on the statistical guideline known as the "one in ten rule",[46] which suggests that the number of observations should be at least ten times the number of independent variables, a sample size of 46 is considered adequate for multiple linear regression models incorporating up to four independent variables. To ensure the robustness and generalizability of the models to unseen data, 10-fold cross-validation was implemented during the model fitting process using the scikit-learn library. The entire dataset was portioned into 10 subsets. In each iteration, 9 subsets were used for training the model, while the remaining subset was reserved for validation. After each subset had served as the validation set, the average of the validation results was calculated to assess the overall model performance.

3.3 Kinetic analysis

To further elucidate the linear relationships and distinct leaching behaviors observed among the metal elements, the shrinking core model was employed. The SCM provides a theoretical framework for determining the rate-controlling step in heterogeneous leaching reactions. Pyrolyzed black mass typically exhibits a relatively porous structure, which facilitates internal mass transfer while maintaining particle size integrity. Upon the addition of black mass to the acidic solution, a thin gas film initially forms around the solid particles. However, this gas film is rapidly replaced by a liquid film due to electrical agitation. Within this liquid film, insoluble metal oxides (*e.g.* MgO, Al_2O_3) and contaminants can accumulate on the surface of the transition metal oxides particles, forming an ash layer.

The leaching mechanism starts with the diffusion of sulfuric acid ions through the liquid film to the surface of the ash layer. Subsequently, sulfuric acid penetrates and diffuses through the ash layer to reach the surface of the unreacted core. At the core surface, sulfuric acid reacts with the transition metal oxides, forming soluble products. These products then diffuse through the ash layer and the liquid film, ultimately returning to the bulk solution.

Based on shrinking core model, three potential rate-controlling steps were investigated: surface chemical reaction control, film diffusion control, and ash diffusion control. The corresponding conversion equations for these control mechanisms are presented in eqn (1)–(3).[47,48] These SCM equations indicate that the conversion on the left side is proportional to time. Conversion values were calculated based on the leaching rates.

$$1-(1-X)^{\frac{1}{3}}=k_{c}t \tag{1}$$

$$X=k_{d,l}t \tag{2}$$

$$1-3\times(1-X)^{\frac{2}{3}}+2\times(1-X)=k_{d,s}t \tag{3}$$

where X denotes the leaching rate; k_c is the apparent rate constant for chemical reaction control; $k_{d,l}$ is the apparent rate constant for film diffusion control; $k_{d,s}$ is the apparent rate constant for ash diffusion control.

The Arrhenius equation, shown in eqn (4), describes the temperature dependence of reaction rates in physical chemistry. It has been utilized to determine the chemical reaction rate and calculate the activation energy.[49] When the apparent rate constant of a chemical reaction obeys the Arrhenius equation, its Arrhenius plot is expected to exhibit a linear relationship.[50]

$$\ln(k)=-\frac{E_a}{R}\times\frac{1}{T}+\ln(A) \tag{4}$$

where k is the rate constant; E_a is the activation energy; R is the universal gas constant 8.314 J mol^{-1} K^{-1}; T is the absolute temperature in Kelvin; A is the frequency factor.

4 Results and discussion

4.1 Data preparation

The leaching state was calculated based on eqn (5). In this equation, V and C represent the volume and concentration of the leaching solution at the sampling point, respectively. ω is the mass fraction of the element in the input material, and M represents the total mass of the input material. Leaching efficiency is defined as the leaching state determined for the final liquid sample collected from an experiment.

$$\text{Leaching state LS}=(V\times C)/(\omega\times M) \tag{5}$$

Table 3 summarizes the experimental conditions and the corresponding leaching efficiencies. Overall, the results indicate that leaching efficiency increased with increasing temperature. The highest average leaching efficiency was obtained at 65 °C, as shown in Fig. 2(a).

Fig. 2(b) illustrates the influence of leaching temperature on the leaching efficiencies for individual elements (Al, Fe, Ni, Co, Li, and Mn). Specially, the leaching efficiencies of Al, Fe, Ni, Co increased with increasing leaching temperature up to 65 °C, while the leaching efficiencies of Li and Mn exhibited less sensitivity to temperature variations. The comparatively lower leaching efficiencies observed for Ni and Co may be attributed to the low acid concentration employed and the absence of H_2O_2. The concentration of copper in all samples remained below 1 mg L^{-1} and was therefore not considered further in this study.

Fig. 3(a) illustrates the changes in leaching states of Al, Fe, Ni, Co, Li, and Mn over time during the leaching experiment conducted at 65 °C. The leaching efficiencies of Li and Mn exceeded 95% within a short duration and subsequently remained relatively stable. Similarly, the rate of increase in leaching efficiencies for Al, Fe, Ni, and Co also decreased following an initial period of rapid dissolution. Fig. 3(b) depicts the measured profiles of pH, temperature, electrode potential, and conductivity throughout the leaching process. The leaching process was initiated upon the addition of black mass to the solution. Strong exothermic reactions occurred within the initial three minutes, resulting in a temperature increase exceeding 10 °C. Subsequently, the rate of chemical reaction decreased and the leach solution gradually cooled due to the temperature differential between the leach solution and the surrounding water bath. To eliminate the cooling effect arising from the temperature difference between the water bath and the reaction solution, the target leaching temperature was increased from 45 °C to 55 °C after the temperature reached the peak in one specific experiment. However, comparable leaching efficiencies were achieved in this instance compared to experiments conducted at a constant temperature of 55 °C. Apart from periodic sampling, no other external interruptions were introduced during the leaching experiments.

Table 3 Experimental conditions and average leaching efficiencies

Temperature, °C	25	35	45	50	55	45–55	65	75
Average leaching efficiency %	64.8	66.0	69.2	69.1	71.9	72.5	76.5	76.2

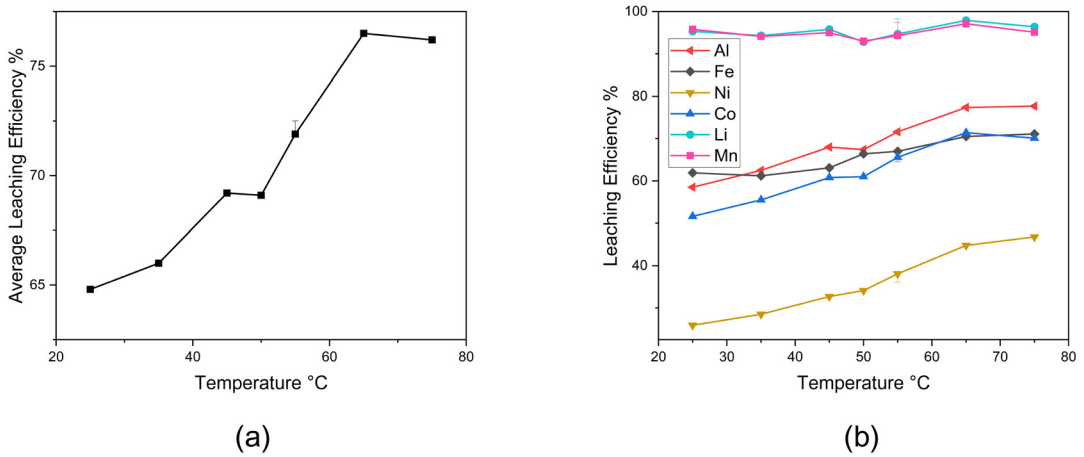

Fig. 2 (a) Temperature influence on overall leaching efficiency; (b) Temperature influence on individual metal elements.

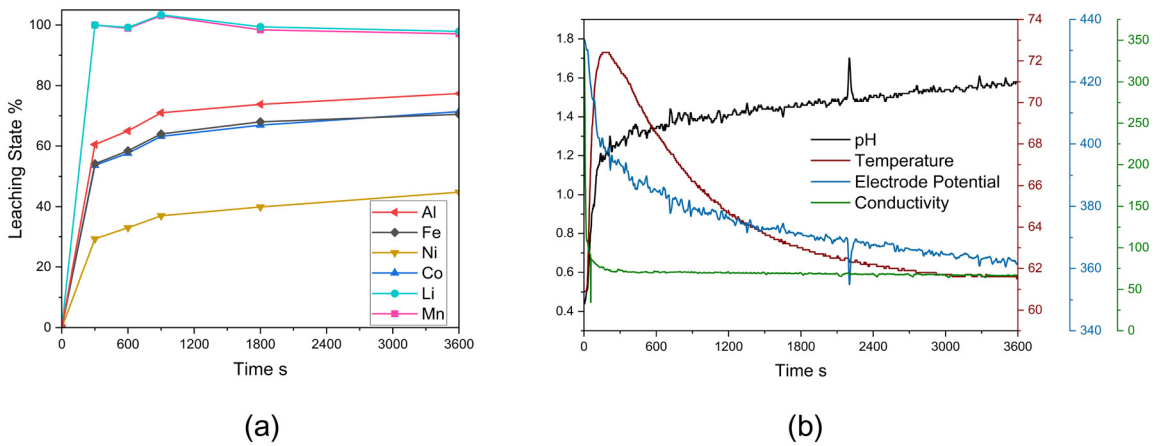

Fig. 3 (a) Metal leaching states at 65 °C; (b) Online sensor data during leaching at 65 °C.

4.2 Correlation analysis

Fig. 4 presents a scatter plot illustrating the relationship between nickel leaching state and pH across different leaching temperatures. A linear trend was observed, with the data points from a single experiment exhibiting a strong linear relationship.

Fig. 5 illustrates the calculated Pearson's and Spearman's correlation matrices based on 38 sampling points. For this analysis, the initial sampling points of each experiment were excluded because they uniformly showed a leaching state of 0%, which would artificially inflate the perceived linear relationship between variables. Correlation coefficients range from −1 to 1. A positive coefficient indicates that two variables tend to increase or decrease together, while a negative coefficient suggests an inverse relationship. The absolute value signifies the strength of the correlation, with values approaching 1 indicating a stronger linear or monotonic relationship.

The leaching states of Al, Fe, Ni, and Co exhibited strong positive correlations with pH values (correlation coefficients > 0.7). Furthermore, the leaching states of Al, Ni, and Co showed strong negative correlations with conductivity. In contrast, the leaching state of Fe displayed a strong negative correlation with electrode potential (mV). The leaching states of Li and Mn exhibited moderate correlations with the electrode potential (correlation coefficients between 0.5 and 0.7).

In addition to the relationships between leaching states and sensor data, the correlation matrix revealed strong correlations

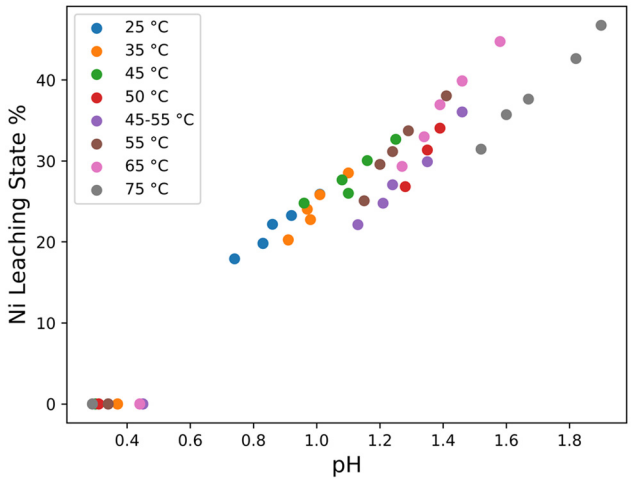

Fig. 4 Scatter plot for leaching state of Ni against pH.

among certain metal ions: Al, Fe, Ni, and Co exhibited high correlations among themselves, as did Li and Mn. These results suggest similar leaching behaviors for Al, Fe, Ni, and Co as a group, distinct from the behaviors of Li and Mn. Additionally, the correlation matrices indicated strong correlations between pH and conductivity, and between both of these variables and temperature. The correlation matrix calculated based on Spearman's rank correlation coefficient yielded results consistent with those obtained using Pearson's correlation.

Both visual inspection and the quantitative correlation analysis indicate that the relationship between online acquired sensor data and the leaching state is not only monotonic, but also potentially linear. However, as correlation analysis intrinsically focuses on the relationship between only two variables, the leaching state may be more accurately described by considering a combination of multiple features.

4.3 Multiple linear regression

4.3.1 Data pre-processing. The data utilized in this study comprise the calculated leaching states of Al, Fe, Ni, Co, Li, and Mn, along with the corresponding pH, temperature, electrode potential, and conductivity obtained from each sample. Variations in temperature across experiments led to distinct ranges in both leaching states and sensor data. Data normalization is a crucial step for eliminating the influence of dimensions, reducing numerical errors, and enhancing model interpretability.[19] To mitigate the effect of temperature variations, data points from each experiment were standardized to the range of [0,1] based on the maximum and minimum values observed within that specific experiment. Compared to normalizing data based on the global maximum and minimum values across all leaching experiments, the individual scaling approach effectively preserves the relative stability of sensor data.

Fig. 4 illustrates a clear shift in pH when examining the unscaled Ni leaching state against the unscaled pH values. This shift is attributed to temperature variations. Following the application of individual scaling, the pH shift was effectively eliminated, resulting in a more accurate fit of the data points to the linear regression model, as shown in Fig. 6(a). Upon rescaling the leaching state, experiments conducted at higher temperatures tend to exhibit higher leaching rates, indicated by steeper slopes (Fig. 6(b)). Nevertheless, the linear relationship between pH and leaching state remains consistent, irrespective of temperature differences. By incorporating individual scaling, the linear regression models can effectively capture this data relationship by adapting the individual scaling factors within the model.

4.3.2 Regression modeling and performance evaluation. Initially, the coefficient of determination (R^2) was used to evaluate the linear regression models. However, most calculated R^2 values exceeded 0.9, which complicated direct comparison between models. As a relative measure of fit, R^2 quantifies the proportion of variance in the dependent variable explained by the independent variables. It does not indicate bias and can be sensitive to the range of the dependent variable. Consequently, the root mean squared error (RMSE), was adopted as the primary evaluation criterion. RMSE quantifies the absolute error between the model's predictions and the actual values, expressed in the same unit as the dependent

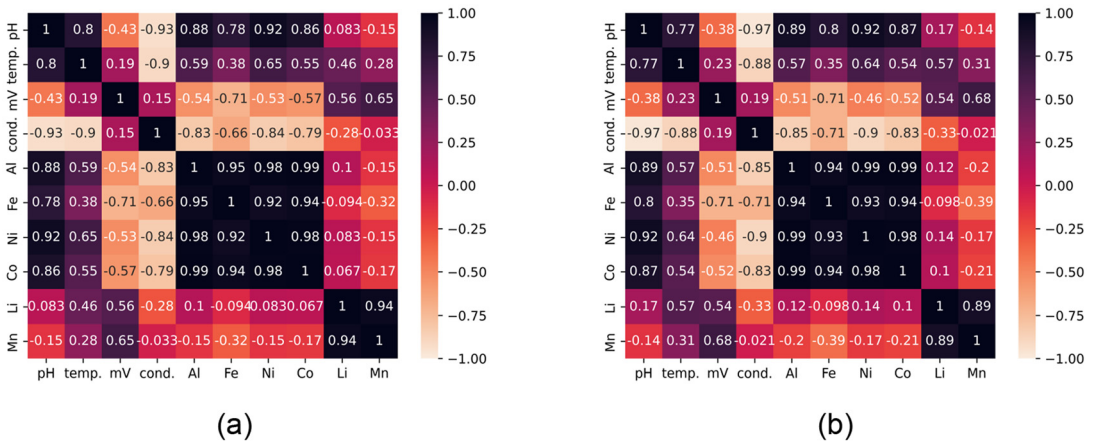

Fig. 5 (a) Pearson's correlation matrix; (b) Spearman's correlation matrix.

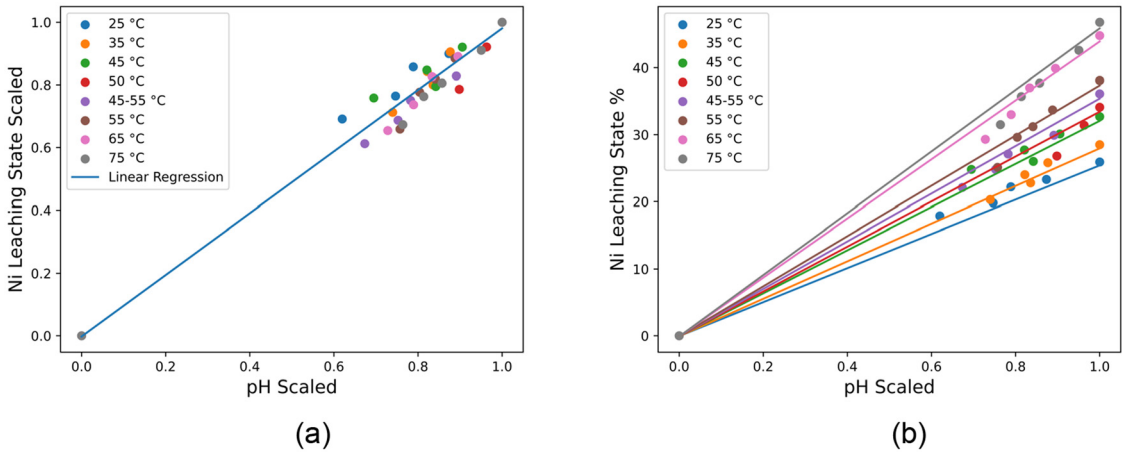

Fig. 6 Linear regression model for Ni using pH as input: (a) Scaled pH and leaching state; (b) Scaled pH and original leaching state.

variable. Following cross-validation, the average RMSE scores of linear regression models with varying input features from the leaching experiments were summarized in Table 4. Models exhibiting only high RMSE scores (exceeding 7) were excluded from further consideration.

pH effectively described the leaching states of Al, Fe, Ni, and Co. However, it proved insufficient for accurately predicting the leaching states of Li and Mn. Conversely, conductivity appeared to be the most effective estimator for the leaching states of Li and Mn, although its predictive power for other metal elements was comparatively lower than that of pH. When temperature was included as a compensatory factor, conductivity could also effectively describe the leaching states of Al, Fe, Ni, and Co. Furthermore, the combination of pH and conductivity yielded the most accurate predictions among the MLR models utilizing two input features. The inclusion of temperature as a third independent variable led to a slight improvement in the performance of the linear regression model.

To assess the influence of training set size on the model's predictive performance, MLR models were trained using data from one, two, three, five, and seven leaching experiments. For each model, pH, conductivity, and temperature were used as input features. This data splitting approach ensured that each training set, regardless of the number of experiments included, contained the complete set of features from all samples collected throughout the duration of the respective leaching processes. A fixed validation dataset, derived from a single leaching experiment conducted at 35 °C, was used consistently for model validation.

Fig. 7 presents the learning curve analysis for the MLR models trained with these varying amounts of data. The training error begins at a low value and increases slightly as more diverse data are added to the training set, eventually tending towards stabilization. Conversely, the validation error starts at a high value and decreases as the model learns from an increasing volume of training data. Both curves subsequently converge at a low error value, with a small gap remaining between them. These observations indicate that the developed MLR model achieves a good bias-variance tradeoff and generalizes well under the evaluated conditions.

The correlation analysis initially indicated a potential linear relationship between sensor data and leaching states. This potential relationship was subsequently corroborated by the linear regression models, as evidenced by the high adjusted R^2 scores and low RMSE values. The data used in this study were derived from samples collected five minutes after the start of

Table 4 Evaluation and comparison of linear regression models using cross-validation

Input feature	Al	Fe	Ni	Co	Li	Mn	Average RMSE
pH	2.9	2.4	1.4	2.8	12.2	12.5	5.7
cond.	4.7	5.1	4.0	4.5	3.1	3.3	4.1
pH & temp.	2.5	2.3	1.3	2.7	5.9	6.2	3.5
mV & temp.	4.7	4.3	2.3	4.7	8.8	9.1	5.7
cond. & temp.	2.1	2.4	1.9	2.3	2.1	2.3	2.2
pH & mV	2.3	2.1	1.4	2.4	5.9	5.8	3.3
pH & cond.	1.8	1.9	1.4	2.3	2.2	2.3	2.0
mV & cond.	1.9	2.0	1.8	2.5	2.2	2.3	2.1
pH & cond. & temp.	1.8	1.8	1.5	2.3	2.0	2.2	1.9

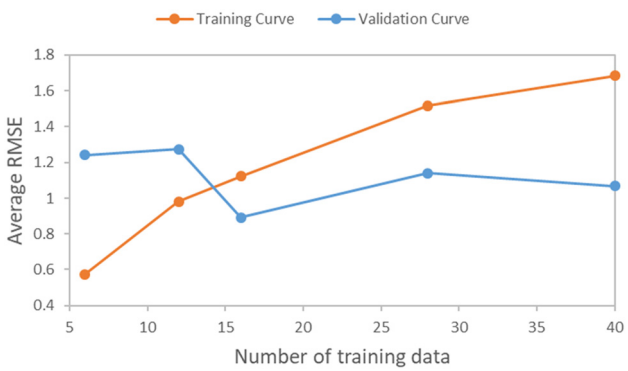

Fig. 7 Learning curve analysis for multiple linear regression models.

the leaching process. The observed linear relationship between sensor data and leaching state may be attributed to the reaction mechanism prevalent during this time period. Furthermore, significant differences in the leaching behavior of different metal elements were observed. The dissolution of Ni and Co proceeded steadily after the initial five minutes and could be accurately estimated using sensor data, whereas the predictive accuracy for Li and Mn remained comparatively lower.

4.4 Kinetic analysis

4.4.1 Determination of the rate-controlling step. In this study, an agitation speed of 450 rpm was employed, which effectively minimized the influence of external diffusion on the mass transfer process. Kinetic analysis focused on data collected starting five minutes after the addition of the black mass. Strong exothermic reactions were captured by sensors during the initial minutes, suggesting that the majority of the chemical reactions between sulfuric acid and black mass particles occurred within this period. It is assumed that, subsequent to this initial period, the rate-controlling step of the dissolution process shifts to the diffusion of reaction products from the particle surface into the bulk solution. Fig. 8 illustrates the plots of conversion against time for Ni and Co, along with corresponding linear regression lines. The slopes of these lines represent the apparent rate constants.

Table 5 summarizes the averaged R^2 scores for all trendlines, considering three potential rate-controlling mecha-

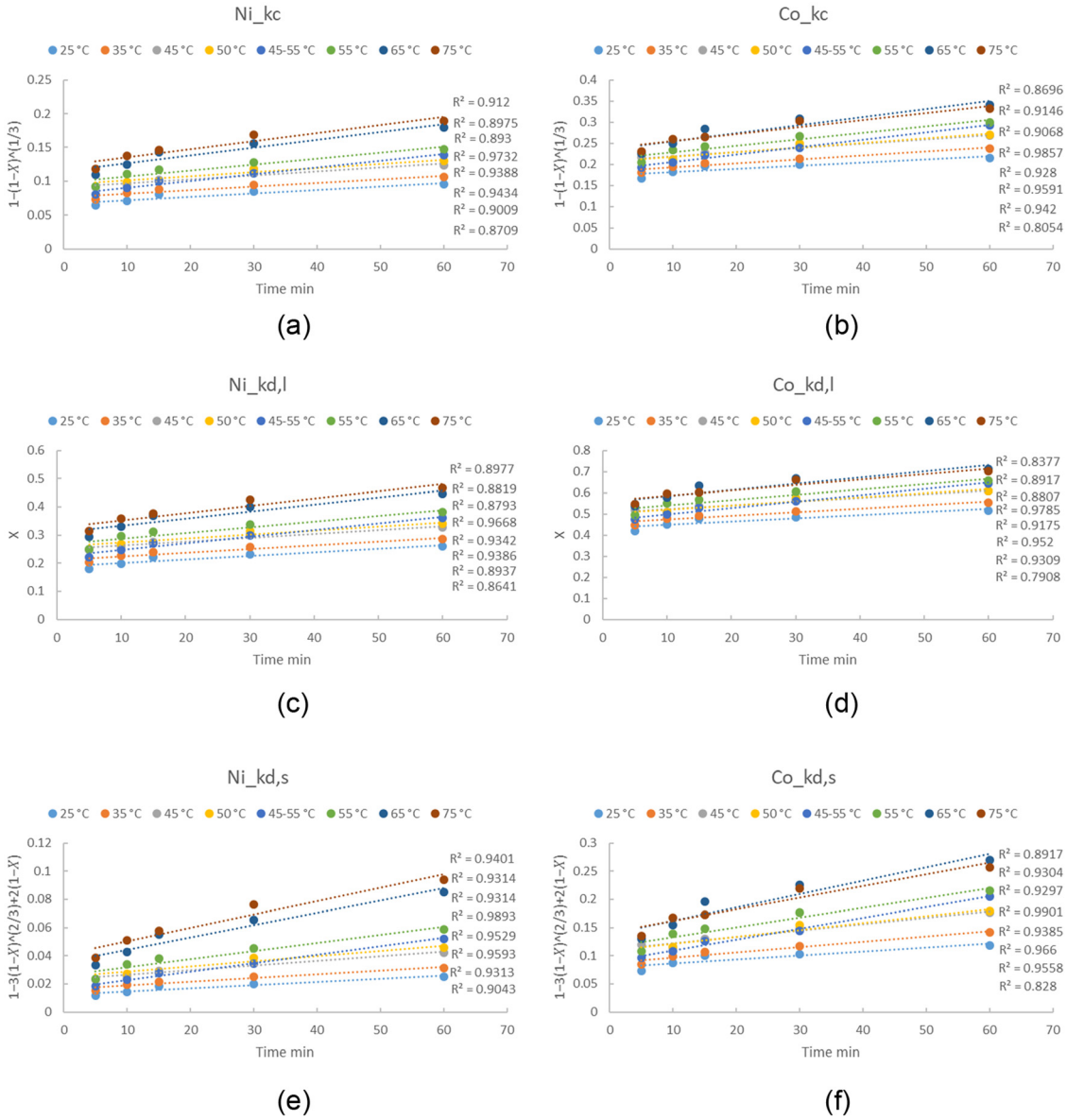

Fig. 8 Plot of SCM equations *versus* time for Ni (a), (c) and (e) and for Co (b), (d) and (f): k_c for chemical reaction control; $k_{d,l}$ for liquid film diffusion control; $k_{d,s}$ for ash diffusion control.

Table 5 Summary of the averaged R^2 scores from all trendlines

	Al	Fe	Ni	Co	Li	Mn
R^2_k_c	0.87	0.86	0.92	0.91	0.38	0.45
R^2_$k_{d,l}$	0.84	0.84	0.91	0.90	0.57	0.71
R^2_$k_{d,s}$	0.89	0.87	0.94	0.93	0.55	0.66
Control mechanism	Ash diffusion	Ash diffusion	Ash diffusion	Ash diffusion	Film diffusion	Film diffusion

nisms for each metal element. The rate-controlling step for each metal element was determined based on the highest R^2 score. Statistical analysis suggests that ash diffusion control is the predominant rate-controlling step for Al, Fe, Ni, and Co, while film diffusion control appears to be the dominant mechanism for Li and Mn. These findings support the hypothesis that a significant amount of newly formed metal sulphate products accumulate on the particle surface after the initial five minutes, hindering further dissolution by restricting the diffusion of products through the ash layer and the surrounding liquid film. Although the results suggest that Li and Mn may have reached the final stages of dissolution due to rapid reaction kinetics, the relatively low R^2 values for these metal elements indicate that the identified control mechanism may not fully explain their leaching behavior. Further investigation is needed to elucidate the precise rate-controlling steps for Li and Mn.

4.4.2 Calculation of the apparent activation energy. Fig. 9 illustrates the Arrhenius plots for Ni, Co, Al, and Fe obtained from black mass leaching experiments. Both fitted lines for Ni and Co exhibit high R^2 scores, indicating a strong linear correlation. However, the R^2 scores for Al and Fe are insufficient for further analysis. The activation energies were determined from the slopes of these lines. The calculated activation energies for Ni and Co were 29.8 kJ mol^{-1} and 22.6 kJ mol^{-1}, respectively. According to previous studies in reaction kinetics, a chemical reaction with an activation energy below 40 kJ mol^{-1} is typically classified as a diffusion-controlled reaction.[51,52] The activation energies for other metal elements were not calculated in this study due to poor linearity in the corresponding plots.

4.5 Leaching state prediction

4.5.1 SCM method. Given the activation energies, the leaching states of Ni and Co at a specific time and temperature can be determined using the Arrhenius equation and the conversion equation of the shrinking core model. Data obtained from the 35 °C leaching experiment were employed as a test set to compare the SCM and the MLR method.

The apparent rate constants $k_{d,s}$ for ash diffusion control were determined using the Arrhenius equation, referred to as eqn (4), yielding values of 0.00027 and 0.00093 for Ni and Co, respectively. These values correspond to the slopes of the trendlines depicted in Fig. 8(e) and (f). The kinetic analysis focused on the leaching process starting from five minutes after its initiation. As the leaching state was not zero at this initial time point, the trendlines required intercepts. In this study, only temperature was varied across all leaching experiments. Therefore, the intercept values are likely related to the leaching temperature. Fig. 10 illustrates the relationship between these intercepts and temperature for both Ni and Co.

The intercept values exhibit a strong positive correlation with leaching temperature, as evidenced by the high R^2 scores obtained from the fitted lines. The equations of these fitted lines were subsequently used to calculate the intercepts specially at a leaching temperature of 35 °C, yielding values of 0.0177 for Ni and 0.0909 for Co. eqn (6) and (7) were then used to calculate the leaching states of Ni and Co. The leaching states of Ni and Co were calculated at the 5, 10, 15, 30, and 60 minutes for the 35 °C experiment and compared with the experimentally determined leaching states at these time points.

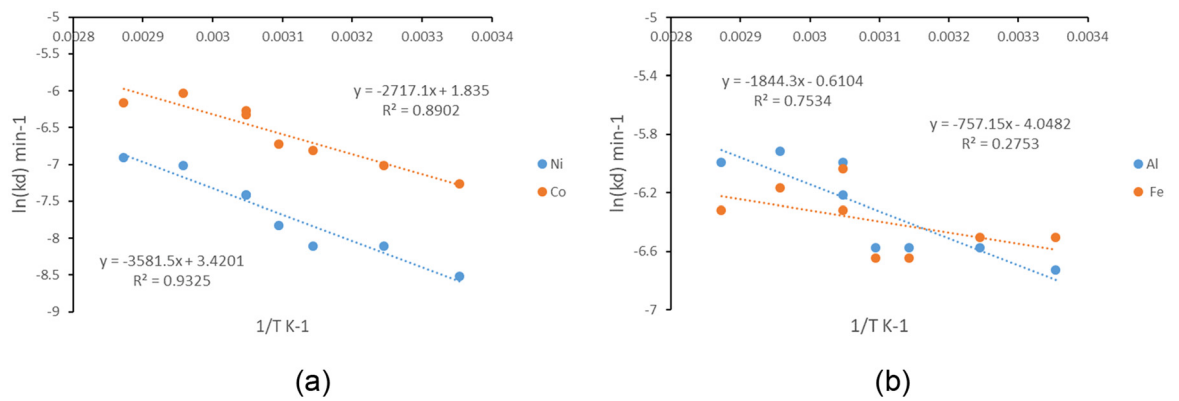

Fig. 9 Arrhenius plot during black mass leaching for (a) Ni, Co and (b) Al, Fe.

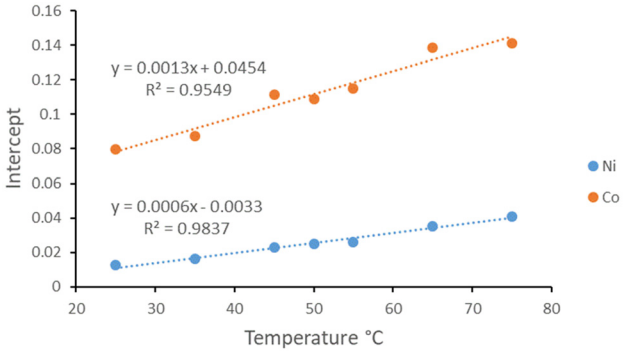

Fig. 10 Trendline intercept and temperature dependency.

$$1 - 3 \times (1 - X_{Ni})^{\frac{2}{3}} + 2 \times (1 - X_{Ni}) = 0.00027 \times t + 0.0177 \quad (6)$$

$$1 - 3 \times (1 - X_{Co})^{\frac{2}{3}} + 2 \times (1 - X_{Co}) = 0.00093 \times t + 0.0909 \quad (7)$$

Here, X_{Ni} denotes the leaching rate for Ni, and X_{Co} represents the leaching rate for Co, with t being the time in minutes.

4.5.2 MLR method. The equations for the best-performing multiple linear regression model are presented in eqn (8)–(13). This model employs pH, conductivity, and temperature as independent variables to predict the metal leaching states.

$$LS_{Al} = 0.42 \times pH - 0.6 \times cond. - 0.08 \times temp. + 0.6 \quad (8)$$

$$LS_{Fe} = 0.54 \times pH - 0.48 \times cond. - 0.08 \times temp. + 0.48 \quad (9)$$

$$LS_{Ni} = 0.71 \times pH - 0.29 \times cond. - 0.11 \times temp. + 0.29 \quad (10)$$

$$LS_{Co} = 0.36 \times pH - 0.65 \times cond. - 0.09 \times temp. + 0.65 \quad (11)$$

$$LS_{Li} = -0.09 \times pH - 1.04 \times cond. + 0.05 \times temp. + 1.04 \quad (12)$$

$$LS_{Mn} = -0.14 \times pH - 1.08 \times cond. + 0.04 \times temp. + 1.08 \quad (13)$$

The equations indicate that both pH and conductivity significantly influence the estimation of the leaching states of Al, Fe, Ni and Co. In contrast, conductivity serves as the primary estimator for the leaching states of Li and Mn. Notably, the equations for Li and Mn exhibit larger intercepts compared to those for the other metals, suggesting a greater influence of factors independent of the input variables included in this model.

4.5.3 Model comparison. The R^2 and RMSE values for the prediction of each element's leaching state were calculated and are summarized in Table 6. Fig. 11 compares the R^2 and RMSE scores for Ni and Co obtained from both the SCM and MLR methods. The MLR method demonstrated better performance in predicting the leaching states of both Ni and Co compared to the SCM. Furthermore, the MLR model possesses the capability to predict the leaching states of Al, Fe, Li, and Mn, which cannot be calculated using the shrinking core model due to the structural limitations of applying this model to the leaching behavior of these elements in the studied material.

The MLR model exhibits strong overall predictive performance, achieving an average adjusted R^2 score of 0.995 and an average prediction error of only 1.1%. This high accuracy is visually corroborated by the close agreement between the predicted and actual leaching states, as illustrated in Fig. 12. Among all metal elements considered, the predictions for Ni and Co exhibit the lowest error rates, suggesting a strong linear relationship between sensor data and their respective leaching states. Conversely, the leaching state predictions for Li exhibit lower accuracy compared to other metal elements, which aligns with the findings of the preceding correlation analysis. Given the empirical nature of this modeling approach, the equations presented above are applicable solely to predicting the leaching state under the specific conditions and when utilizing the same input material, as detailed in Section 2. To apply this modeling approach to other leaching systems or different materials, the model parameters must be adjusted using data obtained from those specific systems.

4.6 Material characterization and its influence on leaching behaviors

Regression modeling demonstrated a strong correlation between sensor measurements and the leaching states of the metal elements. Based on kinetic analysis, this linear relationship can be attributed to the diffusion of metal-ion products through the ash or liquid film layers. However, due to limited linearity in the SCM equations, the statistical data were insufficient to definitively differentiate between the rate-controlling steps for Li and Mn. Furthermore, the applicability of the shrinking core model relies on the assumption that the spherical structure of the metal particles remains intact before and after the leaching process.

To further investigate the distinct leaching behaviors of the metal elements, the thermal pretreatment process of the employed battery black mass was analyzed. Subsequently, scanning electron microscope and energy-dispersive X-Ray spectroscopy (EDS) were employed to characterize the mor-

Table 6 Evaluation of leaching state prediction at 35 °C

	Al	Fe	Ni	Co	Li	Mn	Average
RMSE_SCM	—	—	1.18	1.11	—	—	—
RMSE_MLR	1.07	1.34	0.40	0.33	1.72	1.55	1.07
R^2_SCM	—	—	0.778	0.888	—	—	—
R_{adj}^2_MLR	0.994	0.990	0.996	0.999	0.994	0.995	0.995

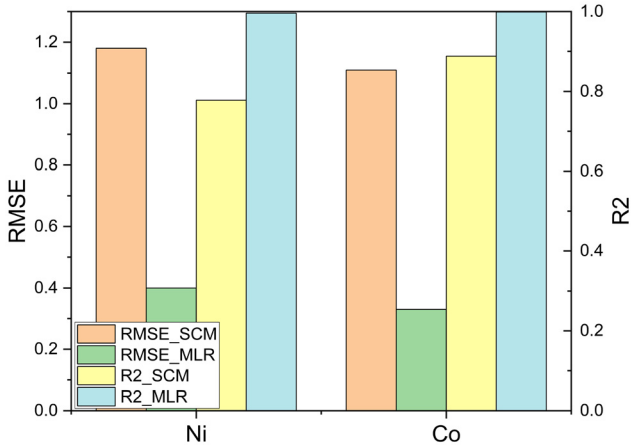

Fig. 11 Comparison of SCM and MLR methods for leaching state prediction.

phology and crystal structure of both the employed black mass and the solid residue obtained after leaching.

4.6.1 Influence of thermal treatment. The black mass utilized in this study was vacuum treated at temperatures between 500 and 550 °C. The observed rapid reaction kinetics for Li and Mn during leaching may be attributed to the effects of this pyrolysis process. During pyrolysis within this temperature range, the layered cathode materials undergo a structural transformation into a spinel structure. Transition metal oxides are initially reduced to simpler mixed oxides such as $LiNiO_2$, $LiCoO_2$, $LiMn_2O_4$, and subsequently further reduced to Li_2O, NiO, CoO, and MnO with the release of oxygen.[53,54] The formation of soluble compounds such as Li_2CO_3 occurs during thermal treatment and is directly related to CO_2 registered during the process.[55] The simplified overall decomposition of cathode materials is summarized in eqn (14) and (15). Possible chemical reactions involved in this process are listed in the following eqn (16)–(23).[56,57]

$$12LiNi_{1/3}Co_{1/3}Mn_{1/3}O_2 + 3C \rightarrow 6Li_2O + 4NiO + 4CoO + 4MnO + 3CO_2 \quad (14)$$

$$12LiNi_{1/3}Co_{1/3}Mn_{1/3}O_2 \rightarrow 6Li_2O + 4NiO + 4CoO + 4MnO + 3O_2 \quad (15)$$

$$4LiNiO_2 + C \rightarrow 2Li_2O + 4NiO + CO_2 \quad (16)$$

$$2LiNiO_2 + C \rightarrow Li_2O + 2NiO + CO \quad (17)$$

$$4LiCoO_2 + C \rightarrow 2Li_2O + 4CoO + CO_2 \quad (18)$$

$$2LiCoO_2 + C \rightarrow Li_2O + 2CoO + CO \quad (19)$$

$$2LiMn_2O_4 + 2C \rightarrow Li_2CO_3 + 4MnO + CO \quad (20)$$

$$6LiMn_2O_4 + 5CO \rightarrow 4Mn_3O_4 + 3Li_2CO_3 + 2CO_2 \quad (21)$$

$$2Mn_2O_3 + C \rightarrow 4MnO + CO_2 \quad (22)$$

$$Li_2O + CO_2 \rightarrow Li_2CO_3 \quad (23)$$

Li_2CO_3 is likely the predominant form of lithium within the pyrolyzed black mass, exhibiting high solubility in sulfuric acid. Lithium dissolution rates were observed to be the fastest, even at lower temperatures, consistent with findings from previous studies.[58,59] This rapid dissolution can be attributed to the absence of a reduction step in the lithium dissolution mechanism.[8,29]

In this study, manganese exhibited faster dissolution rates compared to iron and aluminum. This phenomenon can be explained by the formation of an oxide layer on the surface of iron and aluminum particles, hindering their reaction with sulfuric acid. Among the cathode materials, manganese oxides demonstrated faster dissolution rates compared to cobalt and nickel oxides, likely attributed to their higher standard reduction potential and the formation of more soluble $MnSO_4$. Another contributing factor to the high dissolution rate of manganese is the Jahn–Teller effect. The Jahn–Teller effect is prominent in manganese oxides containing trivalent manganese ions, which induces geometric distortions in the manga-

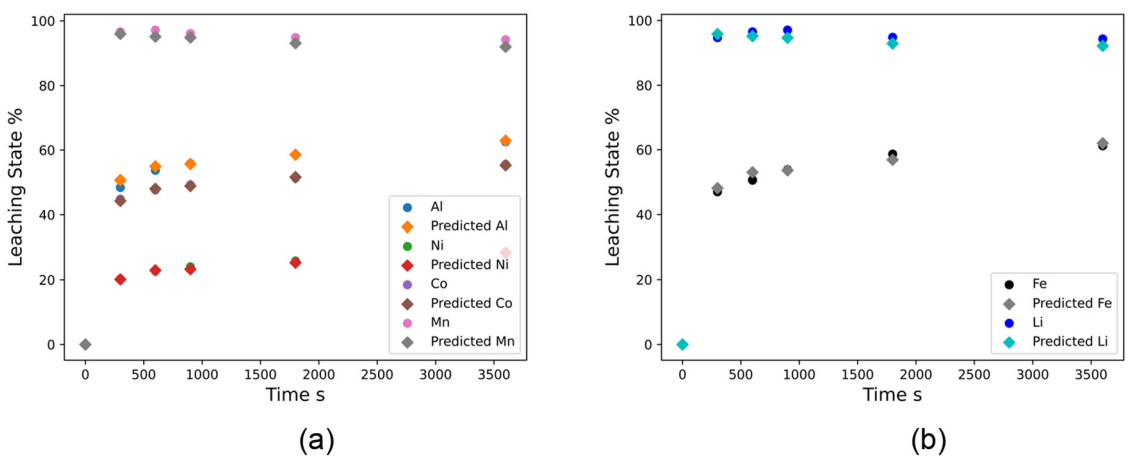

Fig. 12 Visualization of leaching state prediction at 35 °C using MLR model for (a) Al, Ni, Co, Mn (b) Fe, Li.

nese oxide crystal structure, leading to weaker Mn–O bonds and increased instability. As a result, these manganese oxides are more susceptible to acid attack during the leaching process.[50,60,61]

4.6.2 Influence of morphology and crystal structure. Fig. 13 and 14 illustrate SEM images of the pyrolyzed black mass and the solid residue. In these images, heavier elements appear lighter due to differences in electron scattering. EDS analysis was performed to determine the composition of different particles. The results revealed that the light spherical particles correspond to metal oxides originating from the cathode material, while the darker, irregular structures are graphite from the anode material. In the black mass SEM image, spherical particles were observed, distributed either sparsely or in clusters. Quantitative EDS at specific spots on these particles allowed for the differentiation of three distinct types. Type I particles consist primarily of nickel–manganese–cobalt (NMC) oxides, suggesting incomplete decomposition of cathode materials during the pyrolysis process. Type II particles are predominantly manganese oxides (MnO and Mn_2O_3), likely resulting from the further decomposition of $LiMn_2O_4$, as described in eqn (20)–(22). Type III particles consist mainly of nickel and cobalt oxides. A small amount of aluminum was detected within these spherical particles, potentially contributing to the formation of an ash layer during the thermal treatment process. Additionally, impurities such as oxides of Si, Mg, Al, Fe, K were observed attached to the graphite particles.

The SEM image of the solid residue after leaching revealed a higher density of small, light particles. The spherical particles remaining in the residue primarily consisted of nickel and cobalt oxides (Type III), with their shape and size largely unchanged during the leaching process. This observation suggests that the complete consumption of H_2SO_4 by other metal elements resulted in only partial dissolution of nickel and cobalt oxides. Notably, spherical particles containing predominantly manganese oxides were absent in the solid residue, indicating the complete dissolution of these particles. This observation suggests that the SCM theory may not be entirely applicable to manganese, which aligns with the observed low statistical fit. A small amount of the manganese was found within the transition metal oxide particles due to incomplete dissolution of the NMC oxides. Additionally, fully dissolved manganese, along with cobalt, aluminum, and iron may have been trapped within the filter cake during the filtration process and subsequently recrystallized onto graphite or other metal oxide particles during the drying process. Copper is insoluble in 1 molar H_2SO_4 and thus remained in the solid residue.

4.7 Leaching predictive models

Predictive models, including statistical models, chemical kinetic models, and machine learning models, have been applied to the leaching process of primary and secondary materials, as detailed in Table 7. However, research specially

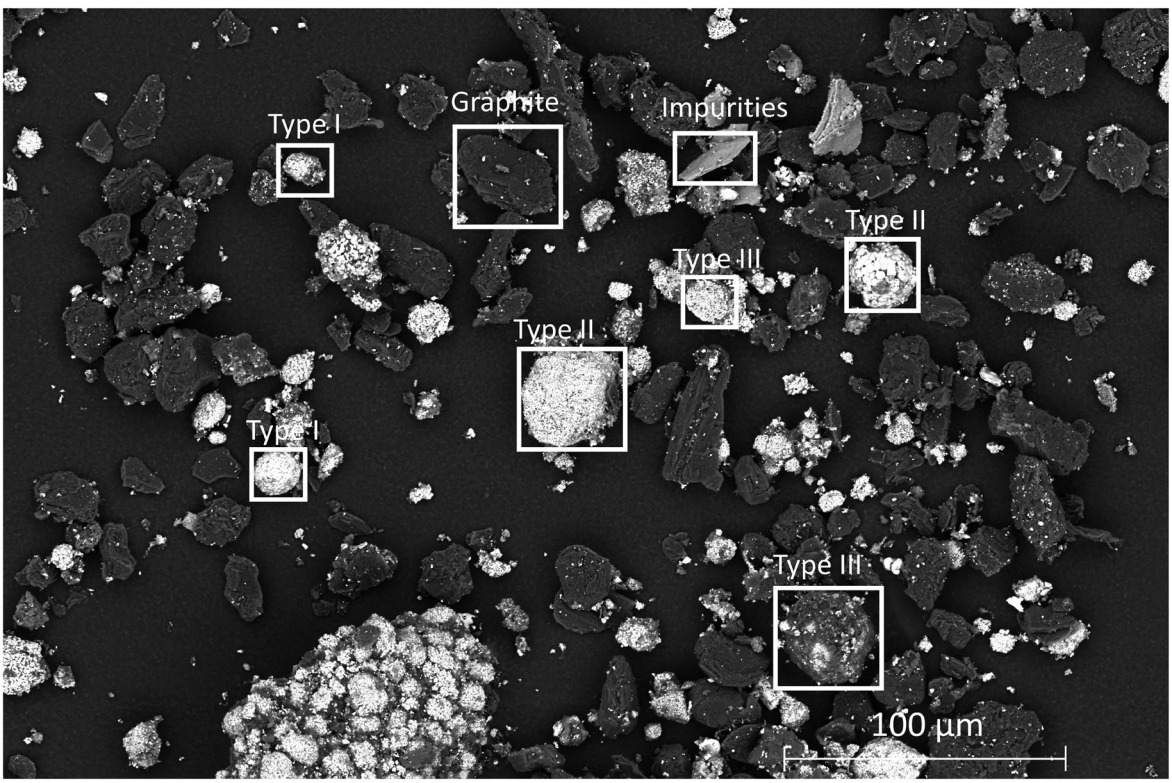

Fig. 13 SEM image of battery black mass before leaching.

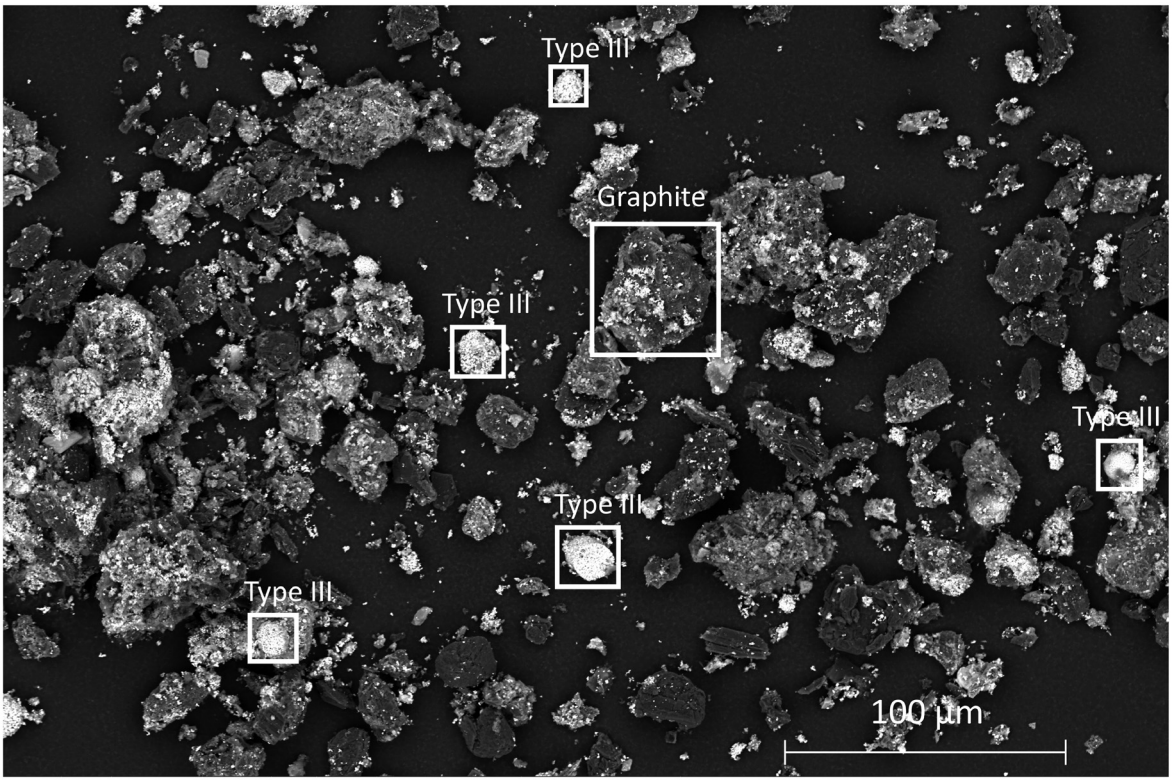

Fig. 14 SEM image of solid residue after leaching.

Table 7 Leaching predictive models and model comparison

Material	Solvent	Predictive models	Data volume	Model inputs	Model outputs	Best results	References
Spent LIBs	Sulfuric acid	MLR SCM with linear fitting equations	<50	Sensor data	Leaching states of Al, Fe, Ni, Co, Li, Mn	MLR R_{adj}^2 0.995 RMSE 1.1	This work
Spent LIBs	Sulfuric acid	MLR	<50	Experimental conditions	Efficiency of Li, Co	R^2 0.95	Ghassa *et al.*[31]
Spent LIBs	Sulfuric acid	ANN	<1000	Random combinations of kinetic data	Kinetic parameters of Li, Co, Ni, Mn	Accuracy 97.8%	Ebrahimzade *et al.*[8]
WPCBs	Sulfuric acid	Second-order MLR Avrami model with linear fitting equations	<100	Experimental conditions	Efficiency of Cu	Second-order MLR R_{adj}^2 0.9	Hao *et al.*[25]
e-Waste	Nitric acid	Second-order MLR	<100	Experimental conditions	Efficiency of Cu	R_{adj}^2 0.987	Barragan *et al.*[42]
Gold	Ferric chloride	Mechanistic kinetic model	<100	Estimated kinetic data	Leaching state of Au	R^2 0.92	Seisko *et al.*[24]
Cobalt compound ore	Sulfuric acid and sulfurous acid	Mathematical mechanism model with error compensation	<500	Experimental conditions Change of acid concentrations	Total leaching state of ore	RMSE 1.1	Hu *et al.*[62]
Copper oxide ore	Sulfuric acid	Nonlinear fitting model Gompertz kinetic model	<50	Leaching states Time	Leaching states of Cu, Co, Fe	Fitting model R^2 0.98	Apua *et al.*[20]
Eudialyte concentrate	Hydrochloric acid and water	ANN SWR MLR	<50	Experimental conditions	Efficiency of total rare earth elements	ANN RMSE 3.27	Ma *et al.*[63]
Alyssum mural ashes	Sulfuric acid	Second-order MLR SCM equation	<50	Experimental conditions	Efficiencies of Ni, Mg	Second-order MLR R^2 0.985	Houzelot *et al.*[48]

focused on predicting leaching states in battery recycling is limited. Multiple linear regression has been commonly employed in previous studies to examine data relationships and predict leaching efficiency, particularly when the available dataset is small. Nevertheless, the majority of these studies have used static experimental conditions for prediction, thus neglecting the dynamic nature of the leaching process.

Chemical kinetic models have been utilized in previous leaching kinetic studies to determine the rate-controlling step and describe the dissolution rate of metallic elements. However, the predictive capabilities of these models have not been sufficiently evaluated.[20,24,25,48] The coefficient of determination, R^2, does not directly quantify prediction error and should therefore not serve as the sole evaluation metric for regression models. Conversely, the root mean squared error, RMSE, measures the average magnitude of the difference between predicted and actual values, thus providing a more robust evaluation of regression model performance.

The proposed approach utilizes sensor measurements as model inputs and the leaching states of metallic elements as model outputs, thereby accounting for the dynamic conditions of the leaching process. In comparison to predictions derived from traditional kinetic models, this approach avoids the need for intricate material characterization and circumvents structural limitations, while simultaneously providing valuable insights for process monitoring. This study represents a pioneering effort in predicting leaching states using online sensor data during the leaching process of battery black mass.

Data relationships are quantitatively investigated through correlation analysis and multiple linear regression, and are also elucidated by principles of leaching kinetics theory. The performance of the models developed in this study is evaluated using both R^2 and RMSE. The MLR model, using pH, conductivity, and temperature as input variables, demonstrates the capability to predict the leaching state of six metallic elements with the highest adjusted R^2 value and the lowest RMSE. Furthermore, the observed variations in the leaching behaviors of the metallic elements are investigated based on thermal pretreatment mechanisms and material morphology, aspects not typically addressed in other leaching kinetic studies of battery black mass.

The proposed approach exhibits adaptability and can be readily applied to other leaching processes where sensor measurements are accessible. More advanced methodologies, such as machine learning algorithms, can be implemented to streamline the process and address more complex scenarios in future research, contingent on the availability of larger datasets.

5 Conclusion

This study combines correlation analysis and regression modeling to propose a novel approach for predicting leaching states using readily measurable sensor data. Pearson's and Spearman's correlation coefficients were employed to explore the linear relationships between sensor data and the metal leaching state. Regression modeling extended this correlation study by incorporating the effect of feature combinations. Predictions of the leaching sate derived from the multiple linear regression model outperformed the traditional calculation methods based on the Arrhenius equation and shrinking core model theory, achieving an average prediction error of less than 1.1%.

The leaching kinetics of nickel and cobalt were effectively described by the shrinking core model. A strong, chemically controlled reaction phase was observed during the initial minutes following the addition of black mass. Subsequently, the leaching of nickel and cobalt proceeded *via* a diffusion-controlled mechanism. During this diffusion-controlled phase, a strong linear relationship between sensor data and leaching state was observed. The calculated activation energies for nickel and cobalt were 29.8 kJ mol^{-1} and 22.6 kJ mol^{-1}, respectively. Given that aluminum and iron do not possess a spherical structure, their leaching kinetics could not be modeled using the shrinking core model. The rapid reaction kinetics observed for lithium and manganese were attributed to the unique physiochemical properties of their respective metal compounds, which were influenced by the thermal pretreatment. To further investigate the kinetics of lithium and manganese, particularly during the initial five minutes of the reaction, faster sampling methods are required.

Due to the complexity of the leaching process and the inhomogeneity of the materials, the findings of this study are specific to the black mass and the experimental conditions employed. To enhance the generalizability of these findings, future research should systematically vary other parameters, such as acid concentration, solid–liquid ratio, and input material. Nevertheless, this methodology, which integrates statistical analysis of online sensor data with kinetic modeling and material characterization techniques, offers a valuable framework for further research and practical applications in this field. The proposed predictive strategy is applicable to leaching processes involving other types of input materials. The monitoring of leaching operations can be optimized through the systematic analysis and modeling of sensor and experimental data. Such optimization is crucial not only for advancing fundamental research but also for enhancing efficiency in industrial applications.

Conflicts of interest

There are no conflicts to declare.

Data availability

The data supporting this article have been included as part of the ESI.†

Acknowledgements

This work was supported by the German Bundesministerium für Bildung und Forschung (BMBF) in the frame of the project "DiRectION", grant number 03XP0358C.

References

1 B. K. Biswal, B. Zhang, P. T. M. Tran, J. Zhang and R. Balasubramanian, Recycling of spent lithium-ion batteries for a sustainable future: recent advancements, *Chem. Soc. Rev.*, 2024, **53**, 5552–5592.
2 J. C.-Y. Jung, P.-C. Sui and J. Zhang, A review of recycling spent lithium-ion battery cathode materials using hydrometallurgical treatments, *J. Energy Storage*, 2021, **35**, 102217.
3 R. Tao, P. Xing, H. Li, Z. Sun and Y. Wu, Recovery of spent LiCoO2 lithium-ion battery via environmentally friendly pyrolysis and hydrometallurgical leaching, *Resour., Conserv. Recycl.*, 2022, **176**, 105921.
4 G. Harper, R. Sommerville, E. Kendrick, L. Driscoll, P. Slater, R. Stolkin, A. Walton, P. Christensen, O. Heidrich, S. Lambert, A. Abbott, K. Ryder, L. Gaines and P. Anderson, Recycling lithium-ion batteries from electric vehicles, *Nature*, 2019, **575**, 75–86.
5 W. Lv, Z. Wang, H. Cao, Y. Sun, Y. Zhang and Z. Sun, A Critical Review and Analysis on the Recycling of Spent Lithium-Ion Batteries, *ACS Sustainable Chem. Eng.*, 2018, **6**, 1504–1521.
6 F. Faraji, A. Alizadeh, F. Rashchi and N. Mostoufi, Kinetics of leaching: a review, *Rev. Chem. Eng.*, 2022, **38**, 113–148.
7 H. S. Fogler, *Elements of chemical reaction engineering*, Prentice-Hall Pearson, Boston, Columbus, Indianapolis, 2016.
8 H. Ebrahimzade, G. R. Khayati and M. Schaffie, Leaching kinetics of valuable metals from waste Li-ion batteries using neural network approach, *J. Mater. Cycles Waste Manage.*, 2018, **20**, 2117–2129.
9 R. W. Missen, C. A. Mims and B. A. Saville, *Introduction to chemical reaction engineering and kinetics*, Wiley, New York, Weinheim, 1999.
10 Y. Zhang, *Geochemical kinetics*, Princeton Univ. Press, Princeton, NJ, 2008.
11 M. A. Reuter, J. van Deventer and T. J. van der Walt, A generalized neural-net kinetic rate equation, *Chem. Eng. Sci.*, 1993, **48**, 1281–1297.
12 M. Fanfoni and M. Tomellini, The Johnson-Mehl- Avrami-Kohnogorov model: A brief review, *Nouv. Cim. D*, 1998, **20**, 1171–1182.
13 K. Shirzad and C. Viney, A critical review on applications of the Avrami equation beyond materials science, *J. R. Soc., Interface*, 2023, **20**, 20230242.
14 P. Schober, C. Boer and L. A. Schwarte, Correlation Coefficients: Appropriate Use and Interpretation, *Anesth. Analg.*, 2018, **126**, 1763–1768.
15 R. J. Hyndman and G. Athanasopoulos, *Forecasting. Principles and practice*, Otexts Online Open-Access Textbook, Lexington, Ky., 2nd edn, 2018.
16 S. D. V. Giakoumatos, C. Siontorou and D. Sidiras, An Extensive Review of Leaching Models for the Forecasting and Integrated Management of Surface and Groundwater Quality, *Water*, 2024, **16**, 3348.
17 C. Aldrich, J. van Deventer and M. A. Reuter, The application of neural nets in the metallurgical industry, *Miner. Eng.*, 1994, **7**, 793–809.
18 R. J. Janse, T. Hoekstra, K. J. Jager, C. Zoccali, G. Tripepi, F. W. Dekker and M. van Diepen, Conducting correlation analysis: important limitations and pitfalls, *Clin. Kidney J.*, 2021, **14**, 2332–2337.
19 F. Zhou, D. Shi, W. Mu, S. Wang, Z. Wang, C. Wei, R. Li and T. Mu, Machine learning models accelerate deep eutectic solvent discovery for the recycling of lithium-ion battery cathodes, *Green Chem.*, 2024, **26**, 7857–7868.
20 M. C. Apua and M. S. Madiba, Leaching kinetics and predictive models for elements extraction from copper oxide ore in sulphuric acid, *J. Taiwan Inst. Chem. Eng.*, 2021, **121**, 313–320.
21 F. Faraji, R. Golmohammadzadeh, F. Rashchi and N. Alimardani, Fungal bioleaching of WPCBs using Aspergillus niger: Observation, optimization and kinetics, *J. Environ. Manage.*, 2018, **217**, 775–787.
22 V. Bewick, L. Cheek and J. Ball, Statistics review 7: Correlation and regression, *Crit. Care*, 2003, **7**, 451–459.
23 M. Lampinen, S. Seisko, O. Forsström, A. Laari, J. Aromaa, M. Lundström and T. Koiranen, Mechanism and kinetics of gold leaching by cupric chloride, *Hydrometallurgy*, 2017, **169**, 103–111.
24 S. Seisko, M. Lampinen, J. Aromaa, A. Laari, T. Koiranen and M. Lundström, Kinetics and mechanisms of gold dissolution by ferric chloride leaching, *Miner. Eng.*, 2018, **115**, 131–141.
25 J. Hao, X. Wang, Y. Wang, Y. Wu and F. Guo, Optimizing the Leaching Parameters and Studying the Kinetics of Copper Recovery from Waste Printed Circuit Boards, *ACS Omega*, 2022, **7**, 3689–3699.
26 S. S. Behera and P. K. Parhi, Leaching kinetics study of neodymium from the scrap magnet using acetic acid, *Sep. Purif. Technol.*, 2016, **160**, 59–66.
27 Y. Yuliusman, R. Fajaryanto, A. Nurqomariah and Silvia, Acid leaching and kinetics study of cobalt recovery from spent lithium-ion batteries with nitric acid, *E3S Web Conf.*, 2018, **67**, 3025.
28 Y. Yuliusman, Silvia, A. Nurqomariah and R. Fajaryanto, Recovery of cobalt and nickel from spent lithium ion batteries with citric acid using leaching process: Kinetics study, *E3S Web Conf.*, 2018, **67**, 3008.
29 W. Xuan, A. de Souza Braga, C. Korbel and A. Chagnes, New insights in the leaching kinetics of cathodic materials in acidic chloride media for lithium-ion battery recycling, *Hydrometallurgy*, 2021, **204**, 105705.
30 L. Xing, J. Bao, S. Zhou, Y. Qiu, H. Sun, S. Gu and J. Yu, Ultra-fast leaching of critical metals from spent lithium-ion

batteries cathode materials achieved by the synergy-coordination mechanism, *Chem. Eng. J.*, 2021, **420**, 129593.
31 S. Ghassa, A. Farzanegan, M. Gharabaghi and H. Abdollahi, The reductive leaching of waste lithium ion batteries in presence of iron ions: Process optimization and kinetics modelling, *J. Cleaner Prod.*, 2020, **262**, 121312.
32 A. R. F. Carreira, A. F. M. Nogueira, I. L. D. Rocha, F. Sosa, A. M. da Costa Lopes, H. Passos, N. Schaeffer and J. A. P. Coutinho, Repurposing Kraft black Liquor as Reductant for Enhanced Lithium-Ion Battery Leaching, *ChemSusChem*, 2024, **17**, e202301801.
33 Z. W. Zhao, W. T. Ding, X. H. Liu and Y. Liang, Effect of ultrasound on kinetics of scheelite leaching in sodium hydroxide, *Can. Metall. Q.*, 2013, **52**, 138–145.
34 T. Makanyire, A. Jha and S. Sutcliffe, Kinetics of hydrochloric acid leaching of niobium from TiO2 residues, *Int. J. Miner. Process.*, 2016, **157**, 1–6.
35 D. Georgiou and V. G. Papangelakis, Sulphuric acid pressure leaching of a limonitic laterite: chemistry and kinetics, *Hydrometallurgy*, 1998, **49**, 23–46.
36 G. Georgalli, J. Eksteen and M. Reuter, An integrated thermochemical-systems approach to the prediction of matte composition dynamics in an Ausmelt® nickel–copper matte converter, *Miner. Eng.*, 2002, **15**, 909–917.
37 Mettler Toledo Group, A Guide to pH Measurement Theory and Practice of pH Applications, **https://www.mt.com/de/en/home/library/guides/lab-analytical-instruments/pH-Theory-Guide.html**.
38 Yokogawa Electric Coporation, "Back to the pHuture" pH and ORP Learning Handbook, **https://web-material3.yokogawa.com/TI12B00A20-01E_pH_Handbook.eu.pdf**.
39 Mettler Toledo Group, A Guide to On-line Conductivity Measurement Theory and Practice, **https://www.mt.com/us/en/home/library/guides/lab-analytical-instruments/Conductivity-Measurement-Theory-Guide.html**.
40 T. H. Lee, Y. K. Chang, B. H. Chung and Y. H. Park, Correlation of redox potential with state variables in cultures under controlled dissolved oxygen concentration and pH, *Biotechnol. Prog.*, 1998, **14**, 959–962.
41 N. May, D. E. Ralph and G. S. Hansford, Dynamic redox potential measurement for determining the ferric leach kinetics of pyrite, *Miner. Eng.*, 1997, **10**, 1279–1290.
42 J. A. Barragan, J. R. A. Castro, A. A. Peregrina-Lucano, M. Sánchez-Amaya, E. P. Rivero and E. R. Larios-Durán, Leaching of Metals from e-Waste: From Its Thermodynamic Analysis and Design to Its Implementation and Optimization, *ACS Omega*, 2021, **6**, 12063–12071.
43 E. Billy, M. Joulié, R. Laucournet, A. Boulineau, E. de Vito and D. Meyer, Dissolution Mechanisms of LiNi1/3Mn1/3Co1/3O2 Positive Electrode Material from Lithium-Ion Batteries in Acid Solution, *ACS Appl. Mater. Interfaces*, 2018, **10**, 16424–16435.
44 F. J. Anscombe, Graphs in Statistical Analysis, *Am. Stat.*, 1973, **27**, 17.
45 W. Song, F. Diaz, A. Yasinskiy, T. Kleinert and B. Friedrich, Enabling data-driven process dynamic modeling for extractive leaching and chemical precipitation, *Chem. Eng. Res. Des.*, 2024, **211**, 179–183.
46 F. E. Harrell, *Regression Modeling Strategies*, Springer International Publishing, Cham, 2015.
47 O. Levenspiel, *Chemical reaction engineering*, Wiley, Hoboken, NJ, 3rd edn, 1999.
48 V. Houzelot, B. Ranc, B. Laubie and M.-O. Simonnot, Agromining of hyperaccumulator biomass: Study of leaching kinetics of extraction of nickel, magnesium, potassium, phosphorus, iron, and manganese from Alyssum murale ashes by sulfuric acid, *Chem. Eng. Res. Des.*, 2018, **129**, 1–11.
49 K. J. Laidler, *Chemical kinetics*, HarperCollins, New York, NY, 3rd edn, 1998.
50 Q. Zheng, M. Watanabe, Y. Iwatate, D. Azuma, K. Shibazaki, Y. Hiraga, A. Kishita and Y. Nakayasu, Hydrothermal leaching of ternary and binary lithium-ion battery cathode materials with citric acid and the kinetic study, *J. Supercrit. Fluids*, 2020, **165**, 104990.
51 I.-H. Lee, Y.-J. Wang and J.-M. Chern, Extraction kinetics of heavy metal-containing sludge, *J. Hazard. Mater.*, 2005, **123**, 112–119.
52 Q. Meng, Y. Zhang and P. Dong, Use of electrochemical cathode-reduction method for leaching of cobalt from spent lithium-ion batteries, *J. Cleaner Prod.*, 2018, **180**, 64–70.
53 C. Stallmeister and B. Friedrich, Holistic Investigation of the Inert Thermal Treatment of Industrially Shredded NMC 622 Lithium-Ion Batteries and Its Influence on Selective Lithium Recovery by Water Leaching, *Metals*, 2023, **13**, 2000.
54 P. Liu, L. Xiao, Y. Tang, Y. Chen, L. Ye and Y. Zhu, Study on the reduction roasting of spent LiNixCoyMnzO2 lithium-ion battery cathode materials, *J. Therm. Anal. Calorim.*, 2019, **136**, 1323–1332.
55 T. Velmurugan, F. Diaz, L. Schwich, M. Keutmann and B. Friedrich, Recyclability study for the next generation of cobalt-free lithium-ion battery systems with C-LNMO, Si/C-LRLO and TiNbO-LNMO active materials via hydrometallurgical route, *J. Power Sources*, 2024, **624**, 235582.
56 S. Balachandran, K. Forsberg, T. Lemaître, N. Vieceli, G. Lombardo and M. Petranikova, Comparative Study for Selective Lithium Recovery via Chemical Transformations during Incineration and Dynamic Pyrolysis of EV Li-Ion Batteries, *Metals*, 2021, **11**, 1240.
57 G. Lombardo, B. Ebin, B.-M. Steenari, M. Alemrajabi, I. Karlsson and M. Petranikova, Comparison of the effects of incineration, vacuum pyrolysis and dynamic pyrolysis on the composition of NMC-lithium battery cathode-material production scraps and separation of the current collector, *Resour., Conserv. Recycl.*, 2021, **164**, 105142.
58 J. Partinen, P. Halli, A. Varonen, B. P. Wilson and M. Lundström, Investigating battery black mass leaching performance as a function of process parameters by combining leaching experiments and regression modeling, *Miner. Eng.*, 2024, **215**, 108828.

59 E. Gerold, R. Lerchbammer and H. Antrekowitsch, Recovery of Cobalt, Nickel, and Lithium from Spent Lithium-Ion Batteries with Gluconic Acid Leaching Process: Kinetics Study, *Batteries*, 2024, **10**, 120.
60 K. Shi, M. Luo, J. Ying, S. Zhen, Z. Xing and R. Chen, Extraction of Lithium from Single-Crystalline Lithium Manganese Oxide Nanotubes Using Ammonium Peroxodisulfate, *iScience*, 2020, **23**, 101768.
61 L. Li, Y. Bian, X. Zhang, Y. Guan, E. Fan, F. Wu and R. Chen, Process for recycling mixed-cathode materials from spent lithium-ion batteries and kinetics of leaching, *Waste Manage.*, 2018, **71**, 362–371.
62 G. Hu, Z. Mao, D. He and F. Yang, Hybrid modeling for the prediction of leaching rate in leaching process based on negative correlation learning bagging ensemble algorithm, *Comput. Chem. Eng.*, 2011, **35**, 2611–2617.
63 Y. Ma, S. Stopic, L. Gronen, M. Milivojevic, S. Obradovic and B. Friedrich, Neural Network Modeling for the Extraction of Rare Earth Elements from Eudialyte Concentrate by Dry Digestion and Leaching, *Metals*, 2018, **8**, 267.